Structural evolution across the insulator-metal transition in oxygen-deficient $BaTiO_{3-\delta}$ studied using neutron total scattering and Rietveld analysis

I.-K. Jeong,[1,*] Seunghun Lee,[2] Se-Young Jeong,[2] C. J. Won,[3] N. Hur,[3] and A. Llobet[4]

[1]*Department of Physics Education & Research Center for Dielectrics and Advanced Matter Physics, Pusan National University, Busan 609-735, Korea*

[2]*Department of Cogno-Mechatronics Engineering, Pusan National University, Miryang 627-706, Korea*

[3]*Department of Physics, Inha University, Incheon 402-751, Korea*

[4]*Los Alamos National Laboratory, Lujan Neutron Science Center, MS H805, Los Alamos, New Mexico 87545, USA*

(Received 15 July 2011; published 29 August 2011)

Oxygen-deficient $BaTiO_{3-\delta}$ exhibits an insulator-metal transition with increasing δ. We performed neutron total scattering measurements to study structural evolution across an insulator-metal transition in $BaTiO_{3-\delta}$. Despite its significant impact on resistivity, slight oxygen reduction ($\delta = 0.09$) caused only a small disturbance on the local doublet splitting of Ti-O bond. This finding implies that local polarization is well preserved under marginal electric conduction. In the highly oxygen-deficient metallic state ($\delta = 0.25$), however, doublet splitting of the Ti-O bond became smeared. The smearing of the local Ti-O doublet is complemented with long-range structural analysis and demonstrates that the metallic conduction in the highly oxygen-reduced $BaTiO_{3-\delta}$ is due to the appearance of nonferroelectric cubic lattice.

DOI: 10.1103/PhysRevB.84.064125 PACS number(s): 77.84.−s, 61.05.fg, 61.43.Gt, 61.50.Ks

I. INTRODUCTION

Oxygen vacancy is one of the common defects in perovskite ferroelectrics[1] and is known to significantly affect electronic transport properties.[2,3] From a structural viewpoint, oxygen vacancies also have an important effect on electric polarization by distorting oxygen cage of a ferroelectric active ion. Thus, it can be speculated that electrical conduction and ferroelectric ordering will be closely related in perovskite ferroelectrics via oxygen deficiency. In fact, a polarization-dependent diode and photovoltaic effect were reported in leaky ferroelectrics such as $BiFeO_3$[4] and $BaTiO_{3-\delta}$.[5]

According to systematic studies on oxygen-deficient $BaTiO_{3-\delta}$ single crystals,[6] an insulator-metal transition occurs with an increase in oxygen vacancies. Across the insulator-metal transition, however, structural distortion caused by oxygen deficiency is not well understood. As itinerant electrons screen Coulombic fields that are responsible for ferroelectric distortions,[7] one may expect that structural distortion disappears in the metallic state, and thus metallic conduction and ferroelectric ordering are not compatible with each other. To investigate crystal symmetry of $BaTiO_{3-\delta}$ in the metallic phase,[8] Kolodiazhnyi *et al*. performed x-ray diffraction studies as a function of temperature. In contrast to the conventional expectation, the authors reported a series of low-symmetry structural transitions in the metallic state and claimed that ferroelectricity persists through the insulator-metal transition of $BaTiO_{3-\delta}$.

We studied the local and long-range structure of $BaTiO_{3-\delta}$ in the insulating and metallic states using neutron total scattering analysis[9] as well as Rietveld refinement. In $BaTiO_3$, an off-centering of the Ti ion with respect to the oxygen octahedron is the source of the local polarization. If the metallic state of $BaTiO_{3-\delta}$ maintains ferroelectricity, then the off-center behavior of Ti ion and an ordering among them should be preserved as well. Thus, local and long-range structural approaches complement each other in understanding structural evolution in oxygen-deficient $BaTiO_{3-\delta}$.

II. EXPERIMENTS AND ANALYSIS

A powder sample of $BaTiO_3$ was synthesized using a conventional solid-state reaction. Oxygen-deficient specimens were obtained by postannealing $BaTiO_3$ powder with Zr foils in a sealed silica tube at 700° (no. 1), 900° (no. 2), and 1100°C (no. 3), respectively. From energy-dispersive x-ray (EDX) spectroscopy, oxygen reduction (δ) of samples 2 and 3 was estimated to be 0.09 and 0.25, respectively. For sample 1, the composition was not reliably differentiated from stoichiometric $BaTiO_3$ using EDX measurement although a comparison of resistivity with that of single-crystal $BaTiO_{2.98}$ suggests that the oxygen reduction will be larger than 0.03. To indicate that sample 1 has almost stoichiometric composition, we will designate it as $BaTiO_3$ (1). Figure 1 shows the electrical resistivity of $BaTiO_{3-\delta}$ as a function of temperature. With increasing reduction of oxygen content, resistivity decreases drastically and temperature-dependent behavior changes from insulating to metallic, consistent with previous studies.[6]

Neutron powder diffraction experiments were performed at room temperature on the neutron powder diffractometer (NPDF) instrument at the Los Alamos Neutron Science Center. For the total scattering analysis, the structure function $S(Q)$ that contains both Bragg and diffuse scattering was determined up to the magnitude of wave vector $Q = 30$ Å^{-1} from neutron powder diffraction measurements after performing corrections for experimental effects and normalization by incident neutron flux using the program PDFgetN.[10] The real-space pair distribution function (PDF) $G(r)$ is obtained by a sine Fourier transform of $S(Q)$ i.e., $G(r) = 4\pi r[\rho(r) - \rho_0] = \frac{2}{\pi}\int_0^{Q_{\max}} Q[S(Q) - 1]\sin Qr\, dQ$. Here, r is the atomic pair distance, and $\rho(r)$ and ρ_0 are the atomic number density and average number density, respectively.

III. RESULTS AND DISCUSSION

Figure 2(a) shows a total scattering structure function, $Q[S(Q) - 1]$, of $BaTiO_3$ (no. 1). The corresponding real-space

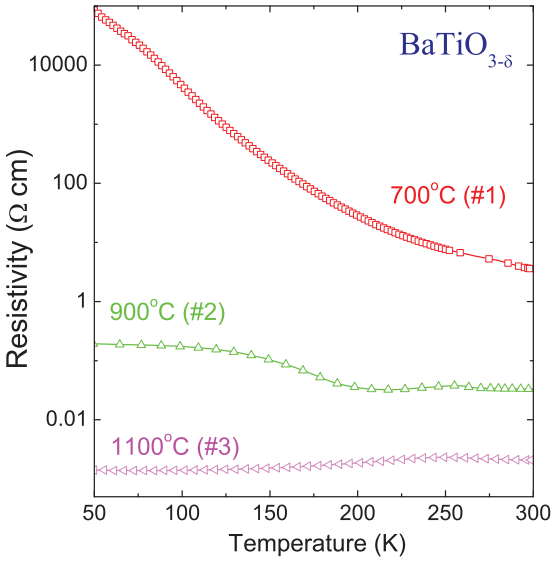

FIG. 1. (Color online) Temperature dependence of resistivity for $BaTiO_{3-\delta}$ samples postannealed in a reduced condition at 700°C, 900°C, and 1100°C, respectively. The resistivity changes from insulating (no. 1, no. 2) to metallic (no. 3) behavior.

PDF spectrum is shown in Fig. 2(b). Here, the first PDF peak appears as a negative peak as the Ti ion has a negative neutron scattering length. Also note that the sixfold degeneracy of the Ti-O bond is broken due to an off-centering of the Ti ion in oxygen octahedron and tetragonal distortion. From the shape

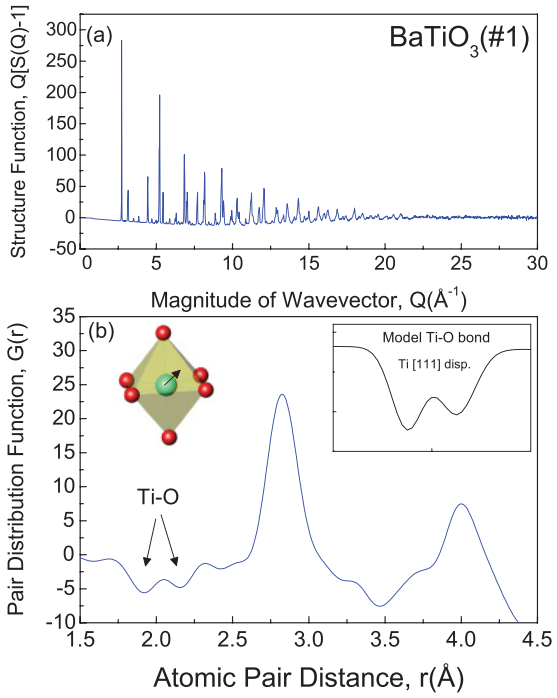

FIG. 2. (Color online) (a) Neutron total scattering structure function, $Q[S(Q)-1]$, of $BaTiO_3$ (no. 1) at 300 K. (b) Corresponding pair distribution function. Note that the first peak appears as a negative peak due to a negative neutron scattering length of the Ti ion. The inset shows the model Ti-O bond length distribution assuming the Ti ion is displaced toward the [111] direction within the oxygen octahedron.

of the well-resolved doublet, we can reasonably speculate that the Ti ion is off-centered toward the [111] direction. For comparison, the inset shows model Ti-O bond length distribution assuming [111] Ti off-centering. As $BaTiO_3$ has a long-range tetragonal structure at room temperature, it is expected that the Ti ion displaces along the [001] direction. However, Ti off-centering along the [001] direction will result in a splitting of the Ti-O bond into one short bond, four medium-length bonds, and one long bond. Thus, the [111] off-centering of the Ti ion found in Fig. 2(b) suggests a discrepancy between the local symmetry of the Ti ion and long-range tetragonal crystal symmetry at room temperature. In fact, x-ray absorption fine-structure measurements[11] as well as first-principles studies[12] showed that the local structure of $BaTiO_3$ remains identical at all temperatures regardless of its long-range average crystal symmetry. Thus, even above the Curie temperature, when the crystal has cubic symmetry, Ti ions are off-centered along eight equivalent ⟨111⟩ directions. With decreasing temperature, these local off-centering develop order-disorder type antiferroelectric coupling[12–15] in one, two, and three dimensions. As a result, the crystal undergoes long-range phase transitions to orthorhombic, tetragonal, and cubic structures, respectively.

Figure 3(a) shows the Ti-O bond length distributions for three samples of $BaTiO_{3-\delta}$. Between $BaTiO_3$ (no. 1) and

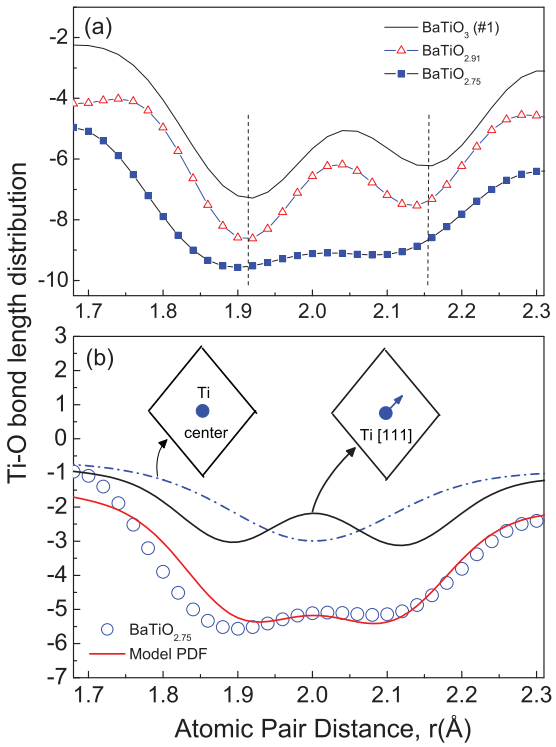

FIG. 3. (Color online) (a) The Ti-O bond length distribution of three $BaTiO_{3-\delta}$ samples. For clarity, distribution functions are shifted vertically from each other. Note that the Ti-O doublet is well resolved in the samples $BaTiO_3$ (no. 1) and $BaTiO_{2.91}$ (insulating) but the splitting became smeared in the metallic $BaTiO_{2.75}$. (b) Comparison of the Ti-O bond length distribution for $BaTiO_{2.75}$ with model calculation. Model Ti-O bond length distribution is composed of two contributions: doublet Ti-O bonds due to Ti [111] displacement and single Ti-O bond with the Ti ion at the center of the octahedron.

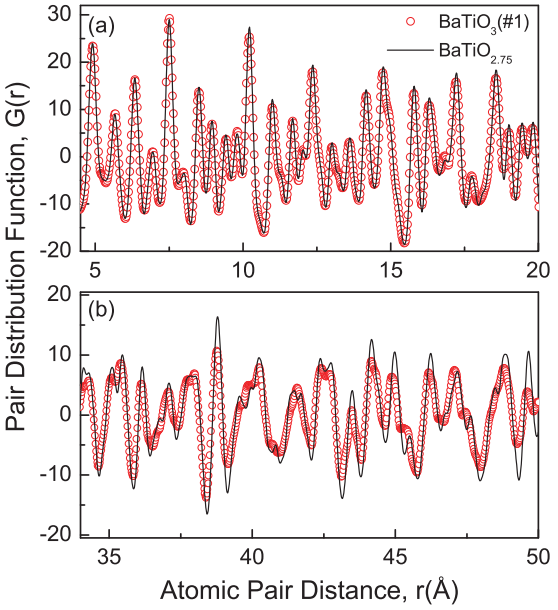

FIG. 4. (Color online) Comparison of the PDF spectra between $BaTiO_3$ (no. 1) and $BaTiO_{2.75}$ in different r ranges. (a) In the r range 3.5 Å $< r <$ 20 Å, both samples have basically identical atomic pair distributions. (b) In a higher r range (34 Å $< r <$ 50 Å), the two PDF spectra become discernible; PDF peaks in the metallic $BaTiO_{2.75}$ are sharper than those in the insulating state.

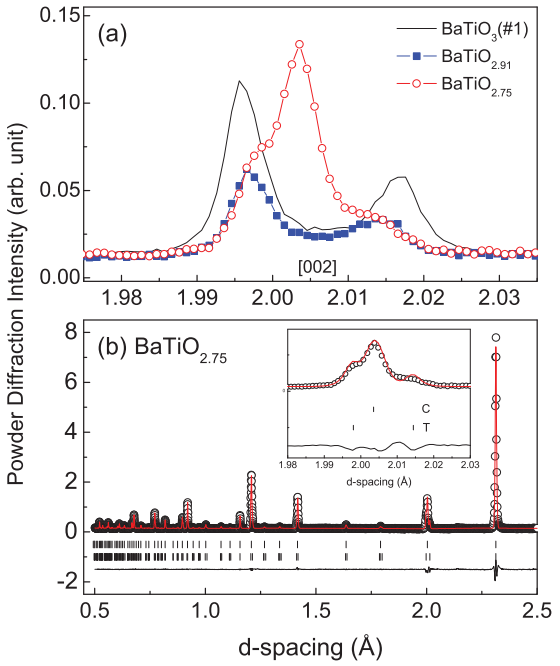

FIG. 5. (Color online) (a) Powder diffraction patterns of $BaTiO_{3-\delta}$ samples. (b) Rietveld fitting of the $BaTiO_{2.75}$. The fit (line) is obtained using mixed tetragonal (T) and cubic (C) phases. The inset shows a part of the fitting around the ⟨200⟩ Bragg peak. Tick marks for cubic and tetragonal phases are shown with a difference curve. Weighted R factor, $R_{wp} = 2.75\%$. In the cubic phase, all atoms sit at high symmetry positions.

$BaTiO_{2.91}$, the Ti-O doublet is little changed although the resistivity is significantly reduced with slight oxygen reduction (Fig. 1). This result implies that local polarization is well maintained under marginal electrical conduction. In contrast, the gap between the two Ti-O peaks is almost completely filled in highly oxygen-deficient $BaTiO_{2.75}$. Figure 3(b) shows a simple model for the smeared Ti-O doublet. The model Ti-O bond length distribution is obtained by assuming two contributions: doublet Ti-O bonds due to Ti [111] displacement and single Ti-O bond with the Ti ion at the center of the octahedron. The reasonable agreement between the experimental and model Ti-O bond distributions suggests that the origin of the smearing may have two distinct phases, one with a distorted Ti-O bond and the other with an undistorted Ti-O bond, as the oxygen deficiency increases.

Beyond the nearest-neighbor Ti-O bond distance, PDF spectra of the insulating $BaTiO_3$(no. 1) and the metallic $BaTiO_{2.75}$ match quite well with each other, as shown in Fig. 4(a). At higher pair distances above $r \sim 35$ Å, however, the two spectra become discernible. In Fig. 4(b), note that PDF peaks of the metallic state are sharper than those in the insulating state. As the PDF peak width represents static and thermal disorder,[16] we expect that highly oxygen-deficient $BaTiO_{2.75}$ will have broader PDF peaks due to structural disorder. However, what we found is that PDF peaks are sharper in disordered $BaTiO_{2.75}$. One plausible explanation is that the average lattice distortion decreases with increasing oxygen reduction.

Finally, we examined the long-range crystal structure of $BaTiO_{3-\delta}$. Figure 5(a) shows part of the neutron powder diffraction pattern near the ⟨200⟩ peak. For the insulating $BaTiO_3$ (no. 1) and $BaTiO_{2.91}$, the cubic ⟨200⟩ peak splits into two Bragg peaks due to the tetragonal distortion. In contrast, the corresponding Bragg peak in the metallic $BaTiO_{2.75}$ shows a three-peak structure that is indicative of a new crystallographic structure.

To obtain detailed long-range structural information, Rietveld refinement was performed for the diffraction patterns of $BaTiO_{3-\delta}$ using GSAS.[17] For $BaTiO_3$ (no. 1) and $BaTiO_{2.91}$, a single tetragonal structure (P4mm) was used for the refinement (not shown). In the case of $BaTiO_{2.75}$, however, a mixed phase of tetragonal (P4mm) and cubic (Pm3m) structures was used, as shown in Fig. 5(b), and an excellent match was obtained. The inset shows the fitting for the Bragg peak near the ⟨200⟩ reflection.

Table I summarizes structural information such as lattice parameters and atomic positions obtained from Rietveld refinement. As discussed earlier, Ti ions are locally off-centered along equivalent ⟨111⟩ directions at all crystal structures. In the average structure refinement, however, we assumed that Ti ion displaces along the [001] direction in the tetragonal structure and stays at the center of the octahedron in the cubic structure.[18] We also tried to refine the occupancy of oxygen content. However, the oxygen occupancy remains close to 1 for all samples, including $BaTiO_{2.75}$. We expect that this result is due to both disorder on the oxygen positions and oxygen occupancy. As both atomic positions and content influence Bragg peak intensities, the oxygen content will not be reliably refined without having good knowledge of oxygen positions. In disordered material like $BaTiO_{2.75}$ we have information only on average atomic positions. Between

TABLE I. Atomic parameters of $BaTiO_{3-\delta}$ obtained from Rietveld refinements. In tetragonal phase, atoms are located at the following sites: Ba at (0,0,0), Ti at (0.5, 0.5, 0.5 + δz_{Ti}), O1 at (0.5, 0.5, δz_{O1}), and O2 at (0.5, 0.0, 0.5 + δz_{O2}).[18] For $BaTiO_{2.75}$, tetragonal-cubic mixed phase fitting was performed. The refined ratio of tetragonal and cubic phases is about 4:6.

		$BaTiO_3$ (no. 1)	$BaTiO_{2.91}$	$BaTiO_{2.75}$	
Space group		P4mm	P4mm	P4mm (41%)	Pm3m (59%)
Lattice	a	3.99307(5)	3.99547(7)	3.99545(5)	4.00700(4)
Parameters (Å)	c	4.03238(6)	4.02744(9)	4.02864(8)	–
Shifts of atoms	δz_{Ti}	0.009(1)	0.013(2)	0.021(1)	0.0
	δz_{O1}	−0.028(1)	−0.025(1)	−0.024(1)	0.0
	δz_{O2}	−0.019(1)	−0.013(2)	−0.008(2)	0.0
R_{wp} (%)		3.27	2.98	2.75	
R_p (%)		2.08	1.91	1.81	

$BaTiO_3$ (no. 1) and $BaTiO_{2.91}$, the tetragonality value of the c/a ratio decreases from 1.010(1) to 1.008(1). However, no further decrease of the c/a ratio was observed in $BaTiO_{2.75}$. It is also worth noting that the displacement of the Ti ion gradually increases with increasing oxygen deficiency. This is an indication of close interplay between oxygen vacancies and Ti displacement. In addition, the two-phase modeling for the highly oxygen-deficient $BaTiO_{2.75}$ showed that the amount of the cubic phase is about 60%. This result complements the local structural finding of the smeared Ti-O doublet [Fig. 3(b)] and suggests an appearance of an average cubic lattice from the tetragonal lattice in $BaTiO_{2.75}$.

IV. CONCLUSION

The neutron total scattering analysis of $BaTiO_{3-\delta}$ showed that local distortion of the Ti-O bond is stable in the insulating state with slight oxygen reduction ($\delta = 0.09$). In highly oxygen-deficient metallic $BaTiO_{2.75}$, however, distorted and undistorted Ti-O bonds were found to coexist. This local structural analysis is complemented with the long-range structural refinement that suggests a mixed phase of tetragonal and cubic structures in $BaTiO_{2.75}$. These structural results provide insight into understanding insulator-metal transitions in $BaTiO_{3-\delta}$ with increasing oxygen deficiency. As shown in Nb-substituted $BaTiO_3$ and $SrTiO_3$, the presence or disappearance of Ti-O distortion crucially influences conduction behavior. For example, the Ti/Nb-O bond is distorted in semiconducting $BaTi_{0.875}Nb_{0.125}O_3$. In contrast, $SrTi_{0.875}Nb_{0.125}O_3$ exhibits metallic behavior with the undistorted Ti/Nb-O bond.[19] Similarly, the two-phase mixture of $BaTiO_{2.75}$ suggests that the metallic conduction is due to the part of the cubic phase with the undistorted Ti-O bond and the remaining ferroelectric tetragonal phase is insulating. Therefore, we conclude that the ferroelectric ordering and metallic conduction are not coexisting phases but are two distinct phases of the material.

ACKNOWLEDGMENTS

This work was supported by the National Research Foundation of Korea Grants No. 2009-0073785 and No. 2010-00001198, funded by the Korean Government (MEST). Neutron diffraction measurements have benefited from the use of NPDF and HIPD at the Lujan Center at Los Alamos Neutron Science Center, funded by DOE Office of Basic Energy Sciences. Los Alamos National Laboratory is operated by the Los Alamos National Security LLC under DOE Contract DE-AC52-06NA25396. The upgrade of NPDF was funded by the NSF through Grant No. DMR 00-76488.

*To whom correspondence should be addressed:Jeong@pusan.ac.kr

[1]D. M. Smyth, Annu. Rev. Mater. Sci. **15**, 329 (1985).
[2]C. N. Berglund and W. S. Baer, Phys. Rev. **157**, 358 (1967).
[3]T. Mihara, H. Watanabe, and C. A. P. de Araujo, Jpn. J. Appl. Phys., Part 1 **33**, 5281 (1994).
[4]T. Choi, S. Lee, Y. J. Choi, V. Kiryukhin, and S.-W. Cheong, Science **324**, 63 (2009).
[5]C. J. Won, Y. A. Park, K. D. Lee, H. Y. Ryu, and N. Hur, J. Appl. Phys. **109**, 084108 (2011).
[6]T. Kolodiazhnyi, Phys. Rev. B **78**, 045107 (2008).
[7]I. A. Sergienko *et al*., Phys. Rev. Lett. **92**, 065501 (2004).
[8]T. Kolodiazhnyi, M. Tachibana, H. Kawaji, J. Hwang, and E. Takayama-Muromachi, Phys. Rev. Lett. **104**, 147602 (2010).
[9]T. Egami and S. J. L. Billinge, *Underneath the Bragg Peaks: Structural Analysis of Complex Materials* (Pergamon Press, Oxford, UK, 2003).
[10]P. F. Peterson, M. Gutmann, T. Proffen, and S. J. L. Billinge, J. Appl. Crystallogr. **33**, 1192 (2000).
[11]B. Ravel, E. A. Stern, R. I. Vedrinskii, and V. Kraisman, Ferroelectrics **206**, 407 (1998).
[12]Q. Zhang, T. Cagin, and W. A. Goddard III, Proc. Natl. Acad. Sci. USA **103**, 14695 (2006).
[13]E. A. Stern, Phys. Rev. Lett. **93**, 037601 (2004).
[14]C. Laulhe, F. Hippert, R. Bellissent, A. Simon, and G. J. Cuello, Phys. Rev. B **79**, 064104 (2009).
[15]I.-K. Jeong, C. Y. Park, J. S. Ahn, S. Park, and D. J. Kim, Phys. Rev. B **81**, 214119 (2010).

[16]I.-K. Jeong, T. W. Darling, J. K. Lee, T. Proffen, R. H. Heffner, J. S. Park, K. S. Hong, W. Dmowski, and T. Egami, Phys. Rev. Lett. **94**, 147602 (2005).

[17]A. C. Larson and R. B. Von Dreele, Report No. LAUR 86-748, 1986 (unpublished).

[18]F. Jona and G. Shirane, *Ferroelectric Crystals* (Dover, New York, 1993).

[19]K. Page, T. Kolodiazhnyi, T. Proffen, A. K. Cheetham, and R. Seshadri, Phys. Rev. Lett. **101**, 205502 (2008).